Engineering Fracture Mechanics 115 (2014) 296–307

Contents lists available at ScienceDirect

Engineering Fracture Mechanics

journal homepage: www.elsevier.com/locate/engfracmech

Unified correlation of in-plane and out-of-plane constraint with fracture resistance of a dissimilar metal welded joint

J. Yang, G.Z. Wang *, F.Z. Xuan, S.T. Tu

Key Laboratory of Pressure Systems and Safety, Ministry of Education, East China University of Science and Technology, Shanghai 200237, China

ARTICLE INFO

Article history:
Received 9 June 2013
Received in revised form 4 November 2013
Accepted 24 November 2013
Available online 28 November 2013

Keywords:
In-plane constraint
Out-of-plane constraint
Dissimilar metal welded joint
Equivalent plastic strain
Fracture resistance

ABSTRACT

In this study, the fracture resistance of a dissimilar metal welded joint was measured by single edge-notched bend specimens with different in-plane and out-of-plane constraints. Based on the area surrounded by the equivalent plastic strain isoline ahead of a crack tip (a unified constraint parameter), a unified correlation of in-plane and out-of-plane constraint with fracture resistance of the dissimilar metal welded joint with local strength mismatch was established. The results show that the unified constraint parameter can characterize combining constraint composed of in-plane, out-of-plane and material constraint (local strength mismatch).

1. Introduction

Constraint is the resistance of a structure against plastic deformation [1]. According to the crack plane, constraint can be divided into two conditions of in-plane and out-of-plane. The in-plane constraint is directly affected by the specimen dimension in the direction of growing crack, i.e. the length of the un-cracked ligament, whilst the out-of-plane constraint is affected by the specimen dimension parallel to the crack front, i.e. the specimen thickness. As constraint can significantly alter the material's fracture resistance, it is important to develop a clear understanding of its effect on the fracture behavior of material. Different fracture constraint parameters and theories, such as K–T [2], J–Q [3,4], J–A_2 [5] and T_Z [6–8], have been developed to characterize and analyze the constraint effect. These parameters were successfully used to quantify the in-plane or out-of-plane constraint separately. However, both in-plane and out-of-plane constraints generally exist in the actual engineering structures. In order to characterize both constraints together, Mostafavi et al. [9–12] have suggested a unified constraint parameter φ which was defined as the size of the plastic region at the onset of fracture normalized by the plastic region size of a standard test:

$$\varphi = \frac{A_c}{A_{ssy}} \tag{1}$$

where A_c is the plastic region area at fracture and A_{ssy} is the reference plastic region area at fracture for a standard specimen in plane strain condition. Unfortunately, the constraint parameter φ has its limitation in characterizing constraint at higher J-integral for ductile material with higher fracture resistance [13]. The authors in the previous study [13] defined a unified constraint parameter A_p by a modified the parameter φ as follows:

* Corresponding author. Tel.: +86 021 64252681; fax: +86 021 64253513.
E-mail address: gzwang@ecust.edu.cn (G.Z. Wang).

0013-7944/$ - see front matter © 2013 Elsevier Ltd. All rights reserved.
http://dx.doi.org/10.1016/j.engfracmech.2013.11.018

Nomenclature

a	crack length
A_2	parameter quantifying second and third term of stress relative to the first term in a cracked elastic–plastic body
A_c	area of the plastic region at fracture
A_p	a new unified parameter for quantifying both in-plane and out-of-plane constraints
A_{PEEQ}	area surrounded by equivalent plastic strain isoline
A_{ref}	area surrounded by equivalent plastic strain isoline at fracture measured in a standard test
A_{ssy}	area of the plastic region at fracture measured in a standard test
B	specimen thickness
E	Young's modulus
h	weld semi-width
J	J-integral
J_C	fracture resistance characterized by J-integral
J_{ref}	fracture toughness measured in a standard test
K	stress intensity factor
M	a constraint parameter caused by material mismatch
Q	a constraint parameter under elastic-plastic condition
S	loading span
T	T-stress constraint parameter under elastic condition
T_Z	factor of the stress-state in 3D cracked body
W	specimen width
α	stain hardening coefficient in Ramberg–Osgood relation
β_g	a parameter by means of the T-stress to quantify geometrical constraint
β_m	a material constraint parameter
β_T	a total constraint parameter
ε_p	equivalent plastic strain
n	strain hardening exponent in Ramberg–Osgood relation
v	Poisson's ratio
σ_0	yield stress
φ	a unified constraint parameter defined by plastic region area

Abbreviations

3D	three-dimensional
CCT	centre-cracked tension
CT	compact tension
DMWJ	dissimilar metal welded joint
FEM	finite element method
FZ	fusion zone
HAZ	heat affected zone
NIZ	near interface zone
PEEQ	equivalent plastic strain in ABAQUS code
SENB	single-edge notched bend
SENT	single-edge notched tension

$$A_p = \frac{A_{PEEQ}}{A_{ref}} \tag{2}$$

where A_{PEEQ} is the areas surrounded by the equivalent plastic strain (ε_p) isolines ahead of the crack tip and A_{ref} is the reference area surrounded by the ε_p isolines in a standard test. This unified constraint parameter has been indentified to be suitable for specimens with different in-plane and out-of-plane constraints (different crack depths a/W, different specimen widths W, different specimen thicknesses B and different loading configurations (SENB, CT, CCT and SENT)) [13,14]. A unified correlation line ($J_C/J_{ref} - \sqrt{A_p}$ line) of in-plane and out-of-plane constraint with fracture toughness of a steel was obtained [14]. However, the results mentioned above were only obtained from a homogeneous material (A508 steel). It is not clear that whether the unified correlation of in-plane and out-of-plane constraint with fracture resistance can be established by using the constraint parameter A_p for the dissimilar metal welded joints (DMWJs) with highly heterogeneous mechanical property (local strength mismatch).

The DMWJ is indispensable part of nuclear structures and has been widely used in primary water systems of pressurized water reactors in nuclear power plants. It is significant for accurate structural integrity assessment if the correlation of constraint with fracture resistance of different cracks in DMWJs was established and the constraint-dependent fracture

resistance or structurally relevant fracture resistance was obtained. However, due to the highly heterogeneous microstructure, mechanical property and complex structure and crack geometries in DMWJ, there exists the interaction of geometry constraint (in-plane and out-of-plane constraint) and material constraint (local strength mismatch) in the DMWJ, which will affect the crack-tip stress–strain fields and crack growth resistance of the DMWJ. These increase the difficulty of constraint quantification for DMWJ.

Some researchers have studied the strength mismatch effect on stress–strain fields in weld zones [15–20]. Burstow et al. [15] used boundary layer formulations to investigate the crack tip stress fields in different mismatched cases and established a *J*–*Q*–*M* formulation to examine the crack tip stress fields. Where *J* sets the size scale of the local deformation, the hydrostatic stress parameter *Q* quantifies the level of stress triaxiality over a significant distance and the *M* defines as the amplitude of the difference field to scale the near tip stress field caused by material mismatch. A similar methodology has also been proposed by Thaulow and co-workers [16–19]. A total constraint parameter β_T was defined by Betegon and Penuelas [20] as follows:

$$\beta_T = \beta_m \cdot \sqrt{\frac{a}{h}} + \beta_g \tag{3}$$

where β_m is a constraint parameter defined for the overmatched welded joints to quantify the material mismatching effect on the crack tip stress fields, a is crack length, h is weld semi-width and β_g is a geometry parameter by means of the *T*-stress to quantify geometrical constraint. However, these parameters are mainly used to quantify in-plane or out-of-plane constraint of welded joint which is simplified to be composite of base metal and weld metal. For the heat-affected-zone (HAZ) crack and interface crack in the DMWJs, they are not suitable constraint parameters. And the unified correlation of in-plane and out-of-plane constraint with fracture resistance of DMWJ has not been established.

In this paper, a new Alloy52M DMWJ between A508 ferritic steel and 316L stainless steel in nuclear power plants was used. The *J*-resistance curves and apparent fracture toughness of specimens with different in-plane and out-of-plane constraints for two cracks (A508 heat-affected-zone (HAZ) crack and A508/Alloy52Mb interface crack) located at the weakest region in the DMWJ have been measured by using single edge-notched bend (SENB) specimens. The areas surrounded by the ε_p isolines ahead of crack tips in these specimens were calculated by finite element method (FEM), and the parameter A_p was analyzed as a unified measure of in-plane and out-of-plane constraint for the DMWJ. The unified correlation of in-plane and out-of-plane constraint with fracture resistance of the two cracks in the DMWJ was established.

2. Experimental procedures

To establish unified correlation of in-plane and out-of-plane constraint with fracture resistance of the DMWJ, the fracture resistance of the joint needs to be determined by using specimens with different in-plane and out-of-plane constraints. So fracture tests were conducted by using the SENB specimens with different crack depths (in-plane constraint) and specimen thicknesses (out-of-plane) for the Alloy52M DMWJ.

2.1. Materials of the DMWJ

The Alloy52M DMWJ in present study is the same as that in the previous studies of authors [21–23], which is used for connecting the safe end to pipe-nozzle of the reactor pressure vessel. The pipe-nozzle material is ferritic low-alloy steel (A508), and the safe end pipe material is austenitic stainless steel (316L). The weld was manufactured by applying a buttering technique and the buttering material (Alloy52Mb) as well as weld material (Alloy52Mw) is the same nickel-base alloy, but their fabrication procedures were different. The fabrication procedures of the full scale mock up of the DMWJ were detailed in Refs. [22,23], and the four materials composed of the DMWJ are shown in Fig. 1. The chemical compositions of the four materials are listed in Table 1 [22,23]. The true stress–strain curves at room temperature are shown in Fig. 2, and the measured average mechanical property data are listed in Table 2 [24].

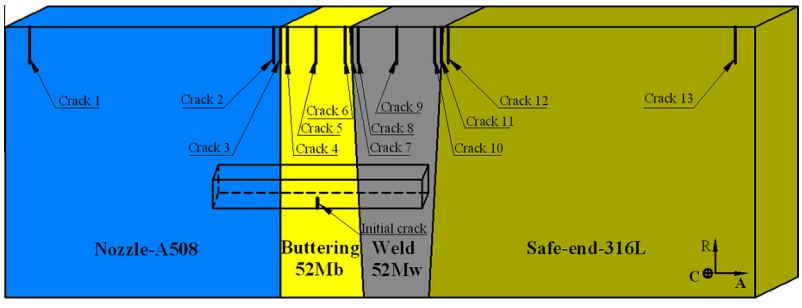

Fig. 1. The four materials composed of the DMWJ and initial crack positions [22,23].

Table 1
Chemical composition of the four materials composed of the DMWJ (Weight%) [22,23].

	C	S	P	Si	Mn	Ni	Cr	Mo	Cu	Al	Ti	Co	Fe	Nb
A508	0.2	0.001	0.005	0.2	1.36	0.96	0.17	0.47	–	–	–	–	Balance	–
52Mb	0.02	<0.001	0.003	0.14	0.25	60.39	28.91	0.01	0.01	0.67	0.56	0.01	9.03	<0.01
52Mw	0.025	0.001	0.004	0.18	0.24	58	29.18	0.01	0.02	0.75	0.53	0.02	10.23	<0.01
316L	0.025	0.001	0.005	0.52	1.73	11.69	17.89	2.43	–	–	–	–	Balance	–

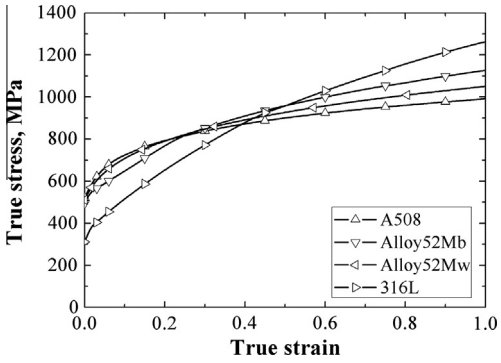

Fig. 2. True stress–strain curves of the four materials at room temperature.

Table 2
Mechanical property data of the four materials at room temperature [24].

Material	Young's modulus E (MPa)	Poisson's ratio v	Yield stress σ_0 (MPa)	Strain hardening coefficient α	Strain hardening exponent n
A508	202410	0.3	522	3.89	7.04
Alloy52Mb	178130	0.3	495	10.73	4.28
Alloy52Mw	178130	0.3	511	7.18	5.42
316L	156150	0.3	311	15.23	2.49

2.2. Specimen geometry

The SENB specimens were machined from the Alloy52M DMWJ, and the specimen orientation is shown in Fig. 1. The two weakest positions (the crack 2 and crack 3, as shown in Fig. 1) with the lowest J-resistance curves [22] were chosen. The crack 2 is located in A508 HAZ with a 1.5 mm distance from A508/52Mb interface, and the crack 3 is located in A508/52Mb interface (Fig. 1). To obtain fracture resistance under different in-plane constraints, the crack 2 and crack 3 specimens (fixed specimen thickness B = 12 mm and width W = 14.4 mm) with five crack depths denoted as a/W = 0.2, 0.3, 0.5, 0.6 and 0.7 were used. To obtain fracture resistance under different out-of-plane constraints, the crack 2 and crack 3 specimens (fixed width W = 14.4 mm and crack depth a/W = 0.5) with five specimen thicknesses denoted as B = 6, 9, 12, 15 and 18 mm were used. The crack 2 and crack 3 specimens with B = 12 mm, W = 14.4 mm (W = 1.2B) and a/W = 0.5 are regarded as standard specimens. The specimen sizes corresponding to the different in-plane and out-of-plane constraints are listed in Table 3. The loading configuration and geometry of the specimens are typically illustrated in Fig. 3 for the crack 2 standard specimen. The loading point and crack are located at the center of the specimen, and the loading span S is 57.6 mm (S = 4W). The specimens were not side-grooved, an initial notch with a length of 5.7 mm was prepared by electro-discharge machining, and then a fatigue pre-crack with a length of about 1.5 mm was made in the specimens.

2.3. Fracture tests

The SENB specimens were tested by an Instron screw-driven machine at room temperature. The quasi-static loading was conducted by displacement controlled mode at a cross-head speed of 0.5 mm/min, and the load-load line displacement curves were automatically recorded by a computer aided control system of the testing machine. The single specimen method and the normalization technique conforming the ASTM E1820 [25] were used to obtain the J-resistance curve for each specimen, which have been described in detail in the previous study [23]. One test was made for each specimen, and the values of the fracture resistance J_C of the specimens with different in-plane and out-of-plane constraints were determined by the 0.2 mm offset lines in the J-resistance curves.

Table 3
Fracture resistance J_C of SENB specimens with different in-plane and out-of-plane constraints.

Crack	W (mm)	a (mm)	a/W	B (mm)	J_C (kJ/m^2)
Crack 2	14.4	2.88	0.2	12	1524.3
	14.4	4.32	0.3	12	837.7
	14.4	7.2	0.5	12	638.8
	14.4	8.64	0.6	12	397.8
	14.4	10.08	0.7	12	263.9
	14.4	7.2	0.5	6	855.2
	14.4	7.2	0.5	9	837.4
	14.4	7.2	0.5	12	638.8
	14.4	7.2	0.5	15	445.4
	14.4	7.2	0.5	18	316.9
Crack 3	14.4	2.88	0.2	12	725.4
	14.4	4.32	0.3	12	588.8
	14.4	7.2	0.5	12	639.3
	14.4	8.64	0.6	12	532.8
	14.4	10.08	0.7	12	409.8
	14.4	7.2	0.5	6	727
	14.4	7.2	0.5	9	669.7
	14.4	7.2	0.5	12	639.3
	14.4	7.2	0.5	15	585.2
	14.4	7.2	0.5	18	491.8

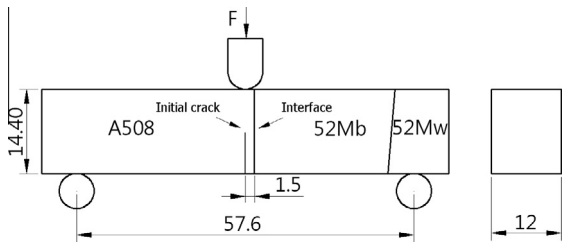

Fig. 3. The loading configuration and geometry of SENB specimen (for the crack 2 standard specimen).

3. Finite element analysis

3.1. Finite element model

The commercial finite element code, ABAQUS, was used to calculate the J-integral and equivalent plastic strain (ε_p) distributions ahead of crack tips. The three-dimensional (3D) finite element (FE) models for the specimens with different in-plane and out-of-plane constraints were built and eight-node isoperimetric elements with reduced integration (C3D8R) were used for all the specimens. The typical FE meshes for the crack 2 standard specimen are illustrated in Fig. 4(a). Since the crack-tip region contains steep stress and strain gradients, the mesh refinement should be more at the crack tip. Thus a conventional mesh configuration having a focused ring of elements surrounding the crack front was used with a small initial root radius (2 μm) at the crack tip (blunt tip) to enhance convergence of the nonlinear iterations, as shown in Fig. 4(b). Fig. 4(b) shows that 16 elements are arranged to surround the crack front, which produces the minimum element size of about 0.4 μm. The mesh sensitivity studies show that when the element number surrounding the crack front is 8, 12 and 16, respectively, the FE results of the J-integral and equivalent plastic strain do not change with the element sizes. The minimum element size of about 0.4 μm in Fig. 4(b) is small enough to get accurate FE results. The typical model in Fig. 4(a) contains 88,840 elements and 10,2447 nodes. The load is applied at the up center of the SENB specimens by prescribing a displacement of 6 mm in the FE modeling. The required J values at different displacement loads can be obtained from the output of ABAQUS. The areas surrounded by the ε_p isolines ahead of crack tips at different J values were calculated.

3.2. Local heterogeneous mechanical properties

The distribution of the local strength along the A508/52Mb interface region is very inhomogeneous due to the heat flow and element diffusion during the welding process [24,26]. This strength mismatch causes material constraint. To incorporate this material constraint (local heterogeneous mechanical properties) into the FE models with different in-plane and out-of-plane constraints, the interface region was divided into three zones: heat affected zone (HAZ) in A508, fusion zone (FZ) and near interface zone (NIZ), as shown in Fig. 5. According to microstructure observation and hardness measurement

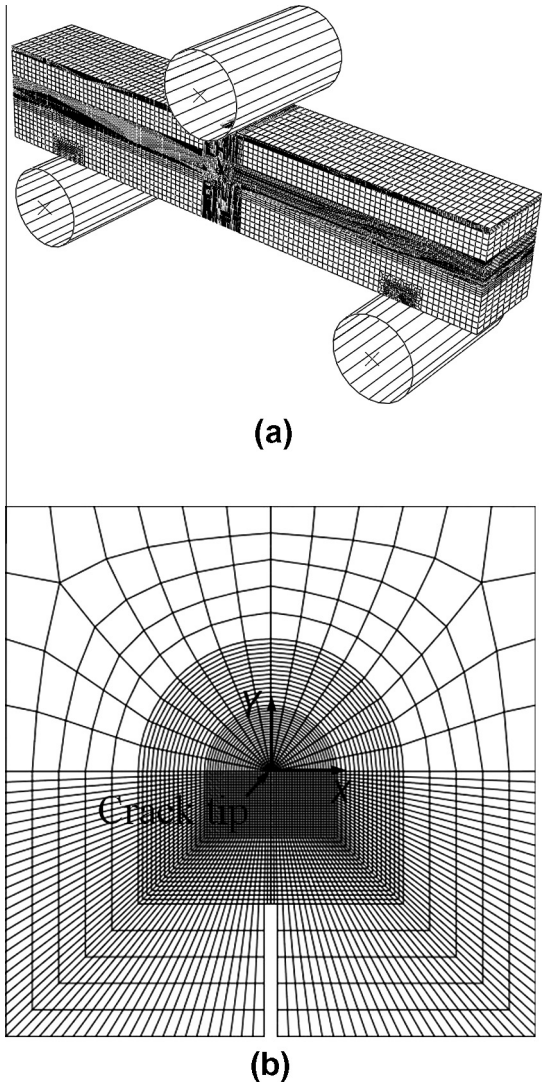

Fig. 4. Typical meshes in the finite element model of specimen (a) and the typical local meshes around the crack tip region (b).

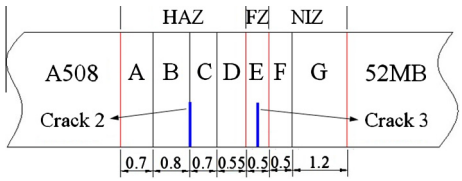

Fig. 5. The A508/52Mb interface region and the initial crack locations.

in our previous work [26], the HAZ and NIZ were further divided into four-material zones (A, B, C and D zones in Fig. 5) and two-material zones (F and G zones in Fig. 5), respectively. The FZ is a single-material E zone. The locations of crack 2 and crack 3 are indicated in Fig. 5 by the[1] blue lines. The local mechanical properties of the DMWJ have been characterized by the mini-sized flat tensile specimens in the previous work of authors [26], and the true stress–strain curves of the A, B, C, D, E, F and G zones at room temperature were taken from the work [26] and reproduced in Fig. 6. The elastic modulus E and Poisson's ratio v for the HAZ, FZ and NIZ are taken to be 180 GPa and 0.3, respectively. The multi-material zones shown in Fig. 5 were modeled in the FE

[1] For interpretation of color in Fig. 5, the reader is referred to the web version of this article.

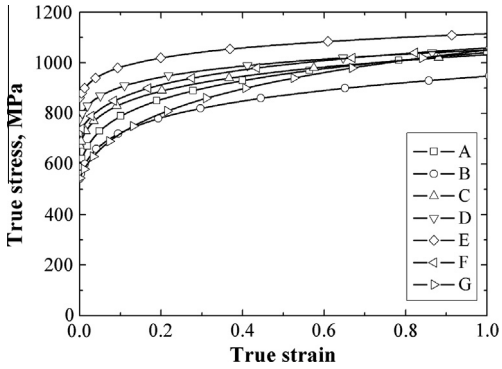

Fig. 6. True stress–strain curves in the A508/52Mb interface region.

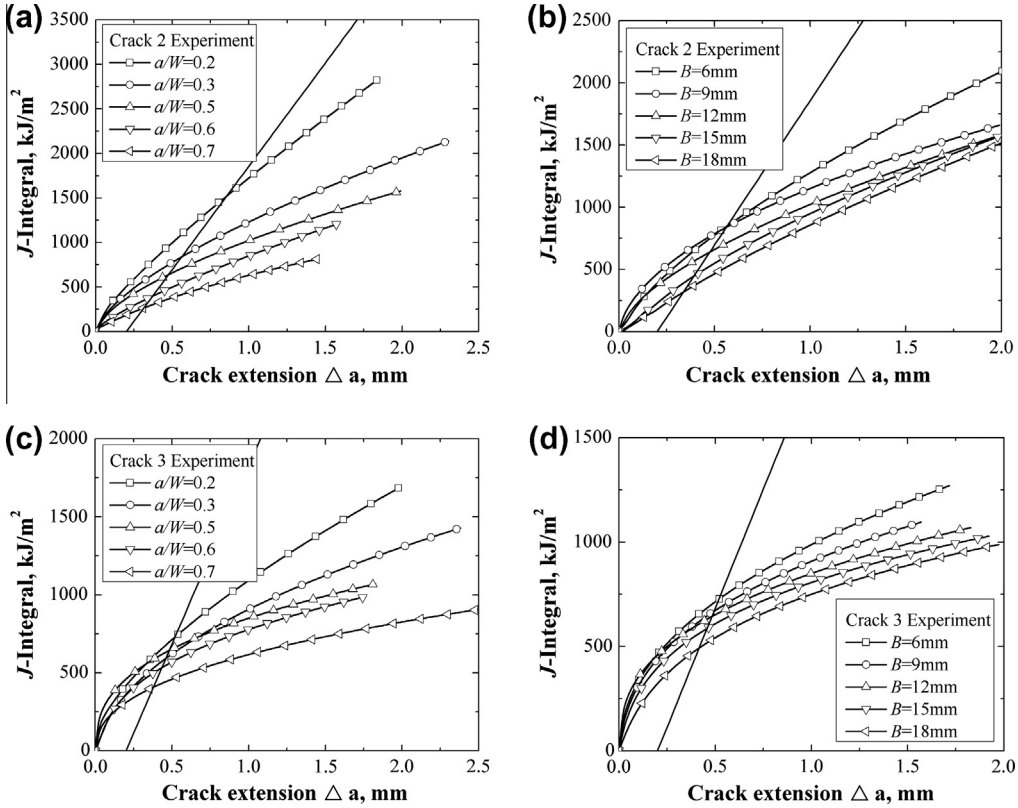

Fig. 7. *J*-resistance curves for crack 2 specimens with different in-plane constraint (a) and out-of-plane constraint (b), and for crack 3 specimens with different in-plane constraint (c) and out-of-plane constraint (d).

models, and the true stress–strain data of each zone in Fig. 6 were used in FE analyses. For the four materials (A508, Alloy52Mb, Alloy52Mw and 316L) beyond the interface region, the elastic–plastic material property data in Fig. 2 and Table 2 were used in FE analyses.

4. Results and discussion

4.1. J-resistance curves and fracture resistance values

Fig. 7 shows the *J*-resistance curves measured for the crack 2 and crack 3 specimens with different in-plane and out-of-plane constraints. It can be seen that the *J*-resistance curves decrease with increasing the in-plane (crack depth) and out-of-plane

constraint (specimen thickness). The fracture resistance values J_C of the different specimens with various in-plane and out-of-plane constraints were determined by the 0.2 mm offset lines in the J-resistance curves and listed in Table 3.

4.2. The areas surrounded by ε_p isolines at different J-integral

To establish unified correlation of in-plane and out-of-plane constraint with the fracture resistance of the DMWJ by using the A_p parameter in Eq. (2), the areas surrounded by the equivalent plastic strain ε_p isolines at different J-integral magnitudes were calculated by FEM in the middle plane of specimens. Figs. 8 and 9 show the areas surrounded by different ε_p isolines (ε_p = 0.2, 0.6 and 1.0) at different J-integral (J = 200 KJ/m^2, 500 KJ/m^2, 1000 KJ/m^2 and 1500 KJ/m^2) for the crack 2 and crack 3 standard specimens, respectively. It can be seen that the distribution of equivalent plastic strain ahead of crack tip is asymmetric due to the local heterogeneous mechanical properties, and the plastic deformation mainly occurs in the material zones with lower yield strength. For the crack 2 specimen in Fig. 8, it can be seen that the areas surrounded by ε_p isolines are small at J = 200 KJ/m^2 and it mainly exists in the zone B with lower strength at the crack tip. With increasing the J-integral, the area surrounded by ε_p isolines increases and the ε_p = 0.2 isoline penetrate different material zones. For example, the ε_p = 0.2 isoline penetrates zone B and enters zone A at J = 1000 KJ/m^2, as shown in Fig. 8(c), and then penetrates zone A and enters A508 and also penetrates zone C and D at J = 1500 KJ/m^2, as shown in Fig. 8(d). However, the ε_p = 0.6 and 1.0 isolines still exist in zone B and zone C. For the crack 3 specimen in Fig. 9, it can be seen that the ε_p = 0.2 isolines gradually penetrate different material zones with increasing the J-integral, but the ε_p = 0.6 and 1.0 isolines mainly exist in zone E and zone F.

Fig. 10(a) and (b) shows the values of A_{PEEQ} (areas surrounded by different ε_p = 0.2, 0.6 and 1.0 isolines) under different J-integral magnitudes for the standard crack 2 and crack 3 specimens, respectively. It can be seen that as the J-integral increases, the A_{PEEQ} surrounded by ε_p = 0.6 and 1.0 isolines essentially monotonously increase, while the A_{PEEQ} surrounded by ε_p = 0.2 isoline increases by a complex nonlinear way for both specimens. The ε_p = 0.2 isoline penetrates different material zones, and the difference in mechanical properties between different zones leads to the complex plastic area (as shown in Figs. 8 and 9). This cause the irregular increase of the area surrounded by ε_p = 0.2 isoline in Fig. 10.

4.3. Unified correlation of in-plane and out-of-plane constraint with fracture resistance

In order to examine whether or not the A_p is a unified measure of in-plane and out-of-plane constraint for DMWJ with material constraint, the A_{PEEQ} values in the middle plane of all specimens with different constraints for different ε_p isolines (ε_p = 0.2, 0.6 and 1.0) ahead of crack tips at $J = J_C$ were calculated (The J_C values are listed in Table 3). The fracture resistance J_C value and the value of A_{PEEQ} at $J = J_C$ of the standard specimens were chosen as the reference toughness J_{ref} and reference area A_{ref}, respectively. After being normalized by the J_{ref} and A_{ref}, the normalized fracture resistance J_C/J_{ref} versus the square root $\sqrt{A_p}$ of the constraint parameter A_p which is calculated by the Eq. (2) for all the specimens can be plotted, as shown in Figs. 11–13.

It can be seen from Fig. 11 that there is a weak monotonic relation between the J_C/J_{ref} and $\sqrt{A_p}$ which is calculated from ε_p = 0.2 isolines for crack 2 and crack 3 specimens with different constraints. From Fig. 12(b), a weak monotonic relation also

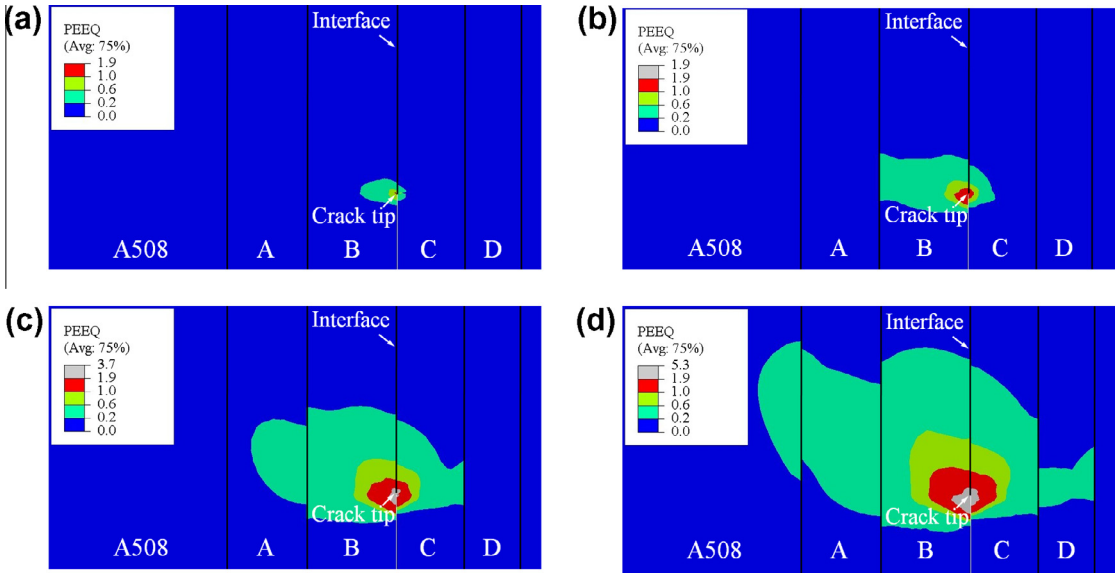

Fig. 8. The equivalent plastic strain (*PEEQ*) contours for crack 2 standard specimen at J = 200 KJ/m^2 (a), J = 500 KJ/m^2 (b), J = 1000 KJ/m^2 (c) and J = 1500 KJ/m^2 (d).

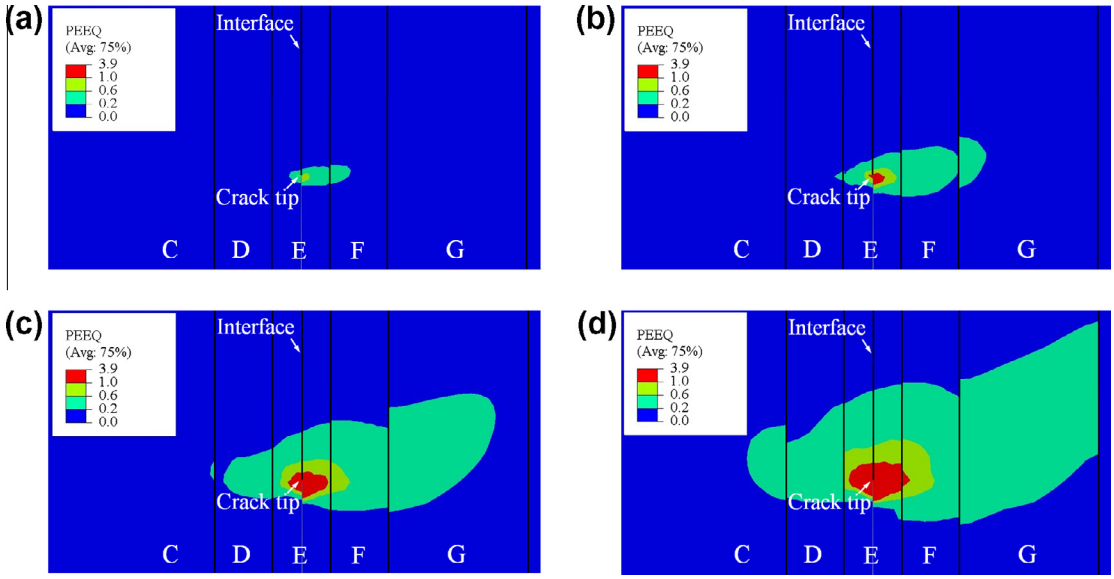

Fig. 9. The equivalent plastic strain (*PEEQ*) contours for crack 3 standard specimen at $J = 200$ KJ/m^2 (a), $J = 500$ KJ/m^2 (b), $J = 1000$ KJ/m^2 (c) and $J = 1500$ KJ/m^2 (d).

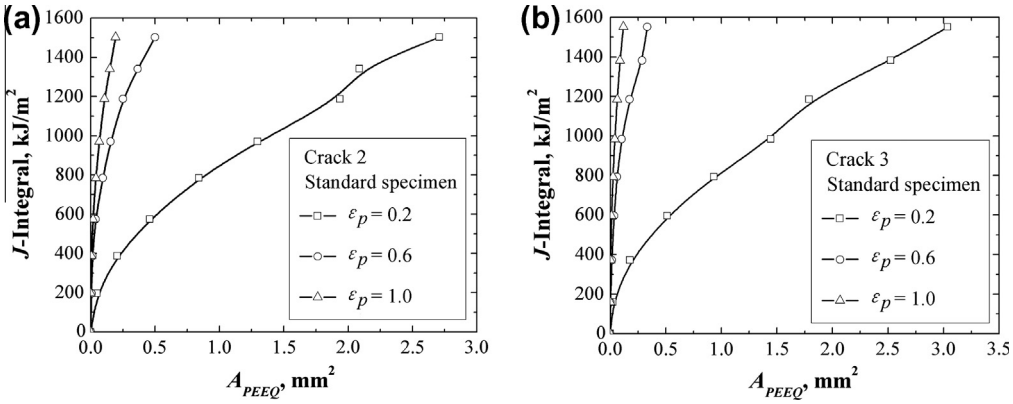

Fig. 10. The areas surrounded by different ε_p isolines under different J-integral magnitudes for crack 2 standard specimen (a) and crack 3 standard specimen (b).

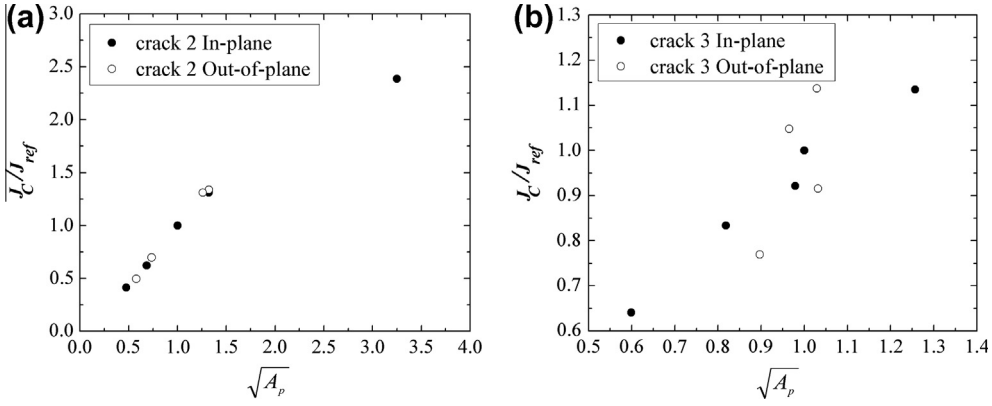

Fig. 11. Normalized fracture resistance J_C/J_{ref} versus the $\sqrt{A_p}$ for the crack 2 specimen (a) and crack 3 specimen (b) obtained from $\varepsilon_p = 0.2$ isoline.

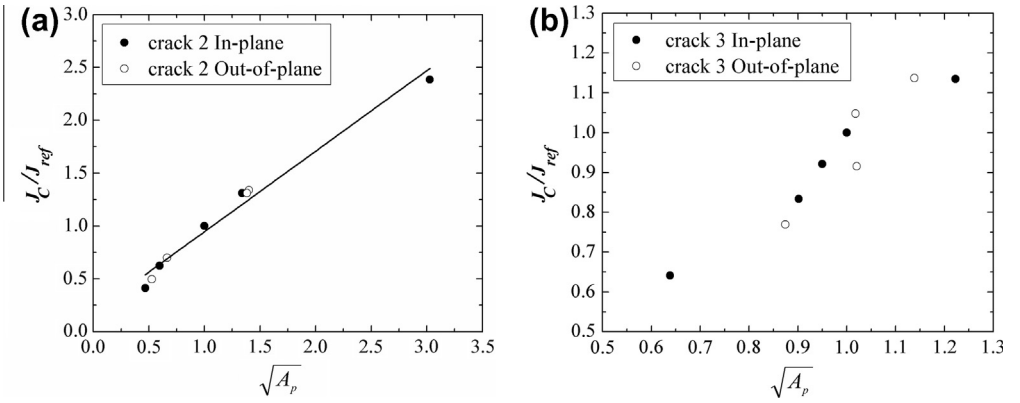

Fig. 12. Normalized fracture resistance J_C/J_{ref} versus the $\sqrt{A_p}$ for the crack 2 specimen (a) and crack 3 specimen (b) obtained from $\varepsilon_p = 0.6$ isoline.

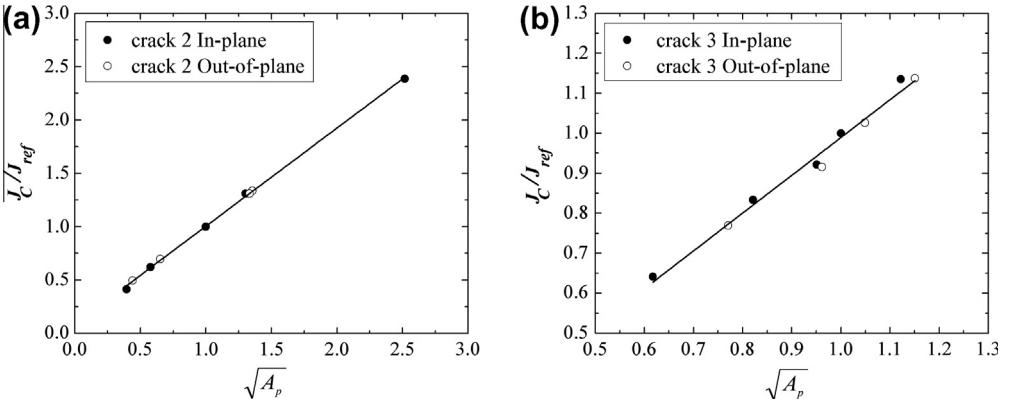

Fig. 13. Normalized fracture resistance J_C/J_{ref} versus the $\sqrt{A_p}$ for the crack 2 specimen (a) and crack 3 specimen (b) obtained from $\varepsilon_p = 1.0$ isoline.

can be found for the $\varepsilon_p = 0.6$ isoline of crack 3 specimen. But a linear relation between the J_C/J_{ref} and $\sqrt{A_p}$ exists for the $\varepsilon_p = 0.6$ isoline of crack 2 specimen regardless of the in-plane and out-of-plane constraints, as shown in Fig. 12(a). Fig. 13 shows that a linear relation between the J_C/J_{ref} and $\sqrt{A_p}$ from $\varepsilon_p = 1.0$ isolines exists for both crack 2 and crack 3 specimens regardless of the in-plane and out-of-plane constraints.

Figs. 11–13 show that the minimum ε_p value for obtaining the unified $J_C/J_{ref} - \sqrt{A_p}$ line for the crack 2 specimen is 0.6, and that for the crack 3 specimen is 1. This may come from the difference in local strength mismatch (material constraint) ahead of crack 2 and crack 3. The degree of local strength mismatch near the interface crack 3 is higher than that near the HAZ crack 2 [26], which can lead to more complex plastic areas surrounded by the lower ε_p isoline in the crack 3 specimen due to the irregular development of plastic deformation (Fig. 9). Thus a higher ε_p value is needed to obtain the unified $J_C/J_{ref} - \sqrt{A_p}$ line for the crack 3 specimens.

The results above show that the A_p is a unified constraint parameter for characterizing both in-plane and out-of-plane constraint of DMWJ with local strength mismatch (local material constraint) when a suitable ε_p value for calculating the area is chosen. With increasing the degree of local strength mismatch near crack, the ε_p value for obtaining the unified $J_C/J_{ref} - \sqrt{A_p}$ line increases. The results also imply that the parameter A_p can characterize both geometry constraint (in-plane and out-of-constraint) and local material constraint (local strength mismatch), while the other constraint parameters described in the introduction cannot characterize these complex constraints. Compared with the total constraint parameter β_T in Ref. [20] which is limited in overmatching and small scale yielding conditions, the A_p can suit for more wide range from small scale to large scale yielding.

Fig. 14 shows the comparison of the $J_C/J_{ref} - \sqrt{A_p}$ lines obtained from $\varepsilon_p = 0.6$ and 1.0 isolines for crack 2 specimen and $\varepsilon_p = 1.0$ and 1.2 isolines for crack 3 specimen. It can be seen that a consistent $J_{IC}/J_{ref} - \sqrt{A_p}$ line is obtained from different ε_p isolines. That is, for the DMWJ, different ε_p isolines above the minimum ε_p value can be selected for calculating the A_p and characterizing the constraint. The study in the previous work [13] shows that the chosen isoline also depends on the material's fracture resistance. With increasing the material's fracture resistance, the magnitude of ε_p being selected as a suitable isoline for calculating the A_p increases. According to the calculation results in present study, for the crack 2 specimen, the $\varepsilon_p \geqslant 0.6$ can be selected; for the crack 3 specimen, $\varepsilon_p \geqslant 1.0$ can be selected.

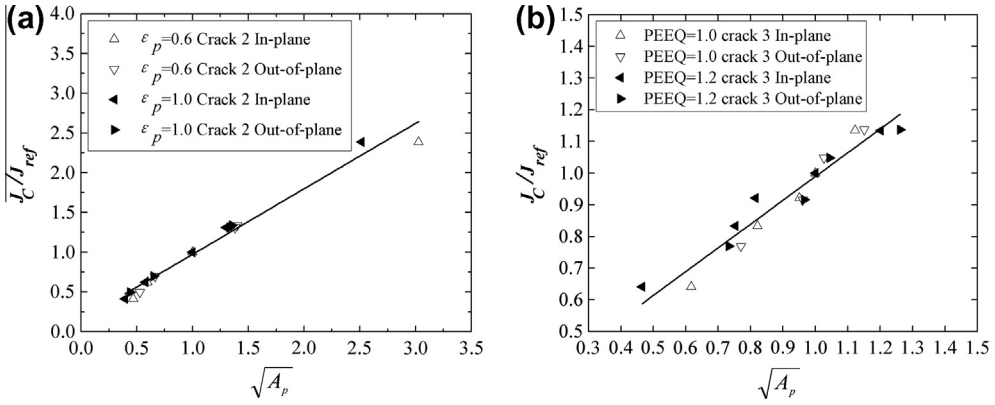

Fig. 14. Comparisons of $J_C/J_{ref} - \sqrt{A_p}$ lines obtained from $\varepsilon_p = 0.6$ and 1.0 isolines for crack 2 specimen (a) and $\varepsilon_p = 1.0$ and 1.2 isolines for crack 3 specimen (b).

The $J_C/J_{ref} - \sqrt{A_p}$ lines in Fig. 14 are unified correlation lines of in-plane and out-of-plane constraint with fracture resistance of DMWJ with different local strength mismatches. It can be used to determine constraint-dependent fracture resistance or structurally relevant fracture resistance. If the reference fracture toughness J_{ref} of standard specimen with high constraint and the unified constraint parameters $\sqrt{A_p}$ of the other specimens or structures are obtained by FEM calculations or experiments, the $J_C/J_{ref} - \sqrt{A_p}$ reference lines (such as in Fig. 14) can be built. It should be noted that the $J_C/J_{ref} - \sqrt{A_p}$ correlation lines in Fig. 14 are based on the SENB specimens with bend loading configuration. Other loading configurations also can impose different constraints at the crack tip. The constraint correlation under the other loading configurations (compact tension, centre-cracked tension and single-edge notched tension) has been studied in the previous study of authors [14] for a homogeneous material (A508 steel). The results show that the unified $J_C/J_{ref} - \sqrt{A_p}$ correlation line also can be obtained under the other loading configurations. For dissimilar metal welded joint in this study, the unified constraint correlation may also be obtained by the other loading configurations.

These unified constraint correlation lines are the constraint-dependent fracture resistance lines of the DMWJ. They may be used in the constraint-dependent fracture assessment for cracked DMWJ components with any complex constraints (in-plane, out-of-plane and material constraints). For a given cracked component, the $J/J_{ref} - \sqrt{A_p}$ line of a crack can be calculated by FE analysis (The J is the applied J-integral for the crack). This $J/J_{ref} - \sqrt{A_p}$ line could be regarded as a constraint-dependent crack driving force line. The intersection of the $J/J_{ref} - \sqrt{A_p}$ line and the $J_C/J_{ref} - \sqrt{A_p}$ line may be the fracture initiation point for the cracked component, and the load corresponding to the $J/J_{ref} = J_C/J_{ref}$ may be the failure load of the component. However, in this constraint-dependent fracture assessment methodology, the determinations of the $J/J_{ref} - \sqrt{A_p}$ line of a cracked component and the $J_C/J_{ref} - \sqrt{A_p}$ line of a material depend on a lot of FEM calculations and tests of specimens with different constraints. These may be the limitations of the methodology. The application of the methodology needs to be further investigated by numerical simulation and experiments.

5. Conclusion

In this study, the fracture resistances of the Alloy52M DMWJ were measured by the SENB specimens with different in-plane and out-of-plane constraints, and the equivalent plastic strain (ε_p) distributions ahead of crack tips in the specimens were calculated by the FEM. Furthermore, the area surrounded by ε_p isoline was analyzed as a unified measure of constraint to obtain the unified correlation of in-plane constraint and out-of-plane constraint with fracture resistance of a DMWJ with local strength mismatch. The main results obtained are summarized as following.

(1) The parameter A_p has a good correlation with the fracture resistance regardless of the levels of the in-plane and out-of-plane constraints in the DMWJ. Different ε_p isolines with higher ε_p values can be selected for calculating the A_p. With increasing the degree of local strength mismatch at crack tip, the magnitude of ε_p being selected as a suitable isoline for calculating the A_p increases.

(2) The A_p may be a unified constraint parameter which can characterize both geometry constraint (in-plane and out-of-constraint) and material constraint (local strength mismatch). There exists a sole linear relation between the J_C/J_{ref} and $\sqrt{A_p}$ regardless of the in-plane and out-of-plane constraint for a crack in the DMWJ. The $J_C/J_{ref} - \sqrt{A_p}$ line is independent on the selection of the ε_p isoline for higher ε_p values, and can be regarded as a unified reference line to characterize the dependence of fracture resistance of a crack in the DMWJ on constraint.

(3) The unified $J_C/J_{ref} - \sqrt{A_p}$ reference lines are the constraint-dependent fracture resistance lines of the DMWJ. They may be used in the constraint-dependent fracture assessment for cracked DMWJ components with any complex constraints (in-plane, out-of-plane and material constraints). This needs to be further investigated.

Acknowledgements

This work was financially supported by the Projects of the National Natural Science Foundation of China (51075149, 51375165 and 51325504) and the Fundamental Research Funds for the Central Universities of China.

References

[1] Brocks W, Schmitt W. The second parameter in *J–R* curves: constraint or triaxiality. In: Constraint effects in fracture: theory and applications: Second Volume. Philadelphia (USA): ASTM STP 1244; 1995.
[2] Larsson SG, Carlsson AJ. Influence of non-singular stress terms and specimen geometry on small-scale yielding at crack tips in elastic–plastic material. J Mech Phys Solids 1973;21:263–77.
[3] O'Dowd NP, Shih CF. Family of crack-tip fields characterized by a triaxiality parameter-I: structure of fields. J Mech Phys Solids 1991;39:989–1015.
[4] O'Dowd NP, Shih CF. Family of crack-tip fields characterized by a triaxiality parameter-II: fracture applications. J Mech Phys Solids 1992;40:939–63.
[5] Chao YJ, Yang S, Sutton MA. On the fracture of solids characterized by one or two parameters: theory and practice. J Mech Phys Solids 1994;42:629–47.
[6] Guo W. Elastoplastic three dimensional crack border field-I: singular structure of the field. Eng Fract Mech 1993;46:93–104.
[7] Guo W. Elastoplastic three dimensional crack border field-II: asymptotic solution for the field. Eng Fract Mech 1993;46:105–13.
[8] Guo W. Elastoplastic three dimensional crack border field-III: fracture parameters. Eng Fract Mech 1995;51:51–71.
[9] Mostafavi M, Smith DJ, Pavier MJ. A micromechanical fracture criterion accounting for in-plane and out-of-plane constraint. Comput Mater Sci 2011;50:2759–70.
[10] Mostafavi M, Pavier MJ, Smith DJ. Unified measure of constraint. ESIA10. Manchester (UK); 2009.
[11] Mostafavi M, Smith DJ, Pavier MJ. Reduction of measured toughness due to out-of-plane constraint in ductile fracture of aluminium alloy specimens. Fatigue Fract Eng Mater Struct 2010;33:724–39.
[12] Mostafavi M, Smith DJ, Pavier MJ. Fracture of aluminium alloy 2024 under biaxial and triaxial loading. Eng Fract Mech 2011;78:1705–16.
[13] Yang J, Wang GZ, Xuan FZ, Tu ST. Unified characterisation of in-plane and out-of-plane constraint based on crack-tip equivalent plastic strain. Fatigue Fract Eng Mater Struct 2012;36:504–14.
[14] Yang J, Wang GZ, Xuan FZ, Tu ST. Unified correlation of in-plane and out-of-plane constraint with fracture toughness. Fatigue Fract Eng Mater Struct 2013. http://dx.doi.org/10.1111/ffe.12094.
[15] Burstow MC, Howard IC, Ainsworth RA. The influence of constraint on crack tip stress fields in strength mismatched welded joints. J Mech Phys Solids 1998;46:845–72.
[16] Thaulow C, Zhang ZL, Hauge M, Burget W, Memhard D. Constraint effects on crack tip stress fields for cracks located at the fusion line of weldments. Comput Mater Sci 1999;15:275–84.
[17] Zhang ZL, Hauge M, Thaulow C. Two parameter characterization of the near tip stress field for a bi-material elastic–plastic interface crack. Int J Fract 1997;79:65–83.
[18] Zhang ZL, Hauge M, Thaulow C. The effect of T stress on the near tip stress field of an elastic-plastic interface crack. In: Advances in fracture research proceedings, ICF 9, vol. 5, 1997. p. 2643–50.
[19] Zhang ZL, Thaulow C, Hauge M. Effects of crack size and weld metal mismatch on the HAZ cleavage fracture toughness of wide plates. Eng Fract Mech 1997;57:653–64.
[20] Betegon C, Penuelas I. A constraint based parameter for quantifying the crack tip stress fields in welded joints. Eng Fract Mech 2006;73:1865–77.
[21] Yang J, Wang GZ, Xuan FZ, Tu ST, Liu CJ. An experimental investigation of in-plane constraint effect on local fracture resistance of a dissimilar metal welded joint. Mater Des 2014;53:611–9.
[22] Wang HT, Wang GZ, Xuan FZ, Tu ST. Fracture mechanism of a dissimilar metal welded joint in nuclear power plant. Eng Fail Anal 2013;28:134–48.
[23] Wang HT, Wang GZ, Xuan FZ, Tu ST. An experimental investigation of local fracture resistance and crack growth paths in a dissimilar metal welded joint. Mater Des 2013;44:179–89.
[24] Wang HT, Wang GZ, Xuan FZ, Liu CJ, Tu ST. Local mechanical properties and microstructures of Alloy52M dissimilar metal welded joint between A508 ferritic steel and 316L stainless steel. Adv Mater Res 2012;509:103–10.
[25] ASTM E1820–08a. Standard test method for measurement of fracture toughness. Philadelphia: American Society for Testing and Materials; 2008.
[26] Wang HT, Wang GZ, Xuan FZ, Tu ST. Local mechanical properties of a dissimilar metal welded joint in nuclear power systems. Mater Sci Eng 2013;568:108–17.